SLAC-PUB-8065
October 2002

# Photocathode rf gun emittance measurements using variable length laser pulses

J.F. Schmerge[a], M. Hernandez[a], M.J. Hogan[a], D.A. Reis[b], H. Winick[a]

[a] Stanford Linear Accelerator Center, Stanford University, Stanford, CA 94309
[b] University of Rochester, Dept. of Physics and Astronomy, Rochester, NY 14627

## Abstract

The Gun Test Facility (GTF) at the Stanford Linear Accelerator Center (SLAC) was created to develop an appropriate injector for the proposed Linac Coherent Light Source (LCLS) at SLAC. The LCLS design requires the injector to produce a beam with at least 1 nC of charge in a 10 ps or shorter pulse with no greater than 1 $\pi$ mm-mrad normalized rms emittance. The first photoinjector under study at the GTF is a 1.6 cell S-band symmetrized gun with an emittance compensation solenoid. Emittance measurements, reported here, were made as function of the transverse laser pulse shape and the Gaussian longitudinal laser pulse length. The lowest achieved emittance to date with 1 nC of charge is 5.6 $\pi$ mm-mrad and was obtained with both a Gaussian longitudinal and transverse pulse shape with 5 ps FWHM and 2.4 mm FWHM respectively. The measurement is in agreement with a PARMELA simulation using measured beam parameters. There are indications that the accelerator settings used in the results presented here were not optimal. Simulations indicate that a normalized emittance meeting the LCLS requirement can be obtained using appropriately shaped transverse and temporal laser/electron beam pulses. Work has begun on producing temporal flat top laser pulses which combined with transverse clipping of the laser is expected to lower the emittance to approximately 1 $\pi$ mm-mrad for 1 nC beams with optimal accelerator settings.

Contributed to Free Electron Laser Challenges II (Technical Conference 3614 of SPIE Photonic West 99 Conf. 26-27 Jan 1999), San Jose, CA.

*Work supported in part by Department of Energy Contract DE-AC03-76SF00515.

# 1. INTRODUCTION

The proposed Linac Coherent Light Source (LCLS)[1,2] at the Stanford Linear Accelerator Center (SLAC) is a single pass, self-amplified spontaneous emission, free-electron laser (FEL) utilizing the last 1 km of the SLAC linac. The last third of the linac is now available since the PEP II B factory utilizes only the first 2 km for injection. A critical component of the LCLS is a high brightness electron source in order to reach saturation in a single pass at 1.5 Å. The source must be able to produce a beam with a least 1 nC, a normalized rms transverse emittance $\leq 1\ \pi$ mm-mrad and a pulse length approximately 10 ps so that the FEL can saturate in an approximately 100 m long wiggler. After acceleration to $\approx 15$ GeV in the last third of the SLAC linac, a 3.4 kA, 1.5 $\pi$ mm-mrad rms, 70 fs rms long pulse would be delivered to the wiggler using two magnetic bunch compressors at 0.3 and 6.0 GeV. The emittance is approximately the diffraction limit ($\gamma\varepsilon_{n\ rms} < \lambda/4\pi$) for 4 Å (3 keV) photons and can also be used to drive single pass FELs at even shorter wavelengths.

The Gun Test Facility (GTF) was constructed to develop an appropriate injector for the LCLS and is located in the Stanford Synchrotron Radiation Lab (SSRL) injector vault at SLAC. The GTF consists of a photo-cathode drive laser, rf power stations, a single 3 m SLAC linac section, rf gun and emittance compensating solenoid as well as electron beam diagnostics to characterize the beam[3,4]. The first gun being characterized at the GTF is the result of a collaboration between Brookhaven National Laboratory (BNL), SLAC and the University of California at Los Angeles. The prototype 1.6 cell gun and emittance compensation solenoid was characterized at BNL[5].

This paper is organized as follows. In Section 2 we describe the experimental set-up and measurement results of the laser pulse length, timing jitter, quantum efficiency (along with an estimate of the thermal emittance), and the projected emittance. The projected emittance measurements reported here are made as a function of laser pulse length and transverse pulse shape. Section 3 describes the GTF laser upgrades and laser pulse shaping experiments underway expected to control the electron beam space charge forces in order to produce lower emittance beams. In Section 4 we present conclusions.

## 2. MEASUREMENTS

### 2.1 Laser

The photocathode drive laser is a chirped-pulse amplification based Nd:glass system. The oscillator is a model GLX-200 from Time-Bandwidth Inc. which is a passively mode-locked diode pumped glass laser. The cavity length of the oscillator determines the repetition rate and has been specifically designed to operate at 119 MHz, the 24th sub-harmonic of the accelerating rf. The oscillator can be tuned from approximately 1050 to 1070 nm. When operated at 1053 nm the laser produced a 250 fs FWHM pulse-length as measured with a Femtochrome Research scanning autocorrelator with a 5.8 nm FWHM bandwidth measured with an Ocean Optics S2000 optical spectrometer. The average power out of the oscillator is 80 mW or 0.7 nJ per pulse. The pulse train from the oscillator is chirped to $\approx$300 ps/nm in a grating pair expander producing positive chirp. A single pulse is then selected at 1.25 or 2.5 Hz for amplification in a Nd:glass regenerative amplifier. After amplification, the 3 mJ, 1053 nm pulse is spatially filtered and then compressed to as short as 1.1 ps FWHM using an adjustable length negative chirp grating pair. One of the compressor gratings is mounted on an optical rail to allow

for quick and repeatable pulse length adjustments by varying the grating separation and thus the compression ratio. The shortest IR pulse produced after amplification and compression is significantly longer than the pulse exiting the oscillator due to gain narrowing (60 round trips in the Nd:glass rod) and bandwidth clipping in the optical stretcher. The IR pulse is then frequency doubled and quadrupled in a 10 mm long, type II, $KD^{*}P$ crystal and a 5 mm long, type I BBO crystal respectively to generate 300 μJ of 263 nm light. The beam diameter in the crystals is $\approx$ 2.4 mm FWHM and typical conversion efficiencies for doubling and quadrupling are 50% and 20% respectively for an overall efficiency of 10%. We typically deliver 200 μJ to the cathode due to various diagnostic pick-offs and transport losses.

The pulse length of the amplified and compressed 1053 nm pulses were measured using an autocorrelator. The minimum pulse length is 1.1 ps FWHM and the pulse length as a function of the compressor spacing is shown in Figure 1. Also shown in Figure 1 is the pulse length of both the 527 and 263 nm pulses which were both measured using a sub-picosecond resolution streak camera. The steak camera used was a Hamamatsu FESCA-500 streak camera with a A1976-01 UV optic set. The streak camera resolution had been previously measured to be 0.5 ps FWHM with a $\approx$100 fs Ti:Sapphire laser pulse.

Pulses as short as 4.6 ps FWHM in the UV were measured and include pulse broadening of $\approx$1 ps due to a spatial chirp across the beam in the compressor dispersion plane. The chirp is evident in both the 527 and 263 nm pulses and is most likely due to a misalignment in the optical compressor. The green and UV pulses typically demonstrate significant pulse broadening near the optimum compression of the IR pulse because the

doubling and quadrupling crystals have not been optimally matched to the IR laser pulse intensity.

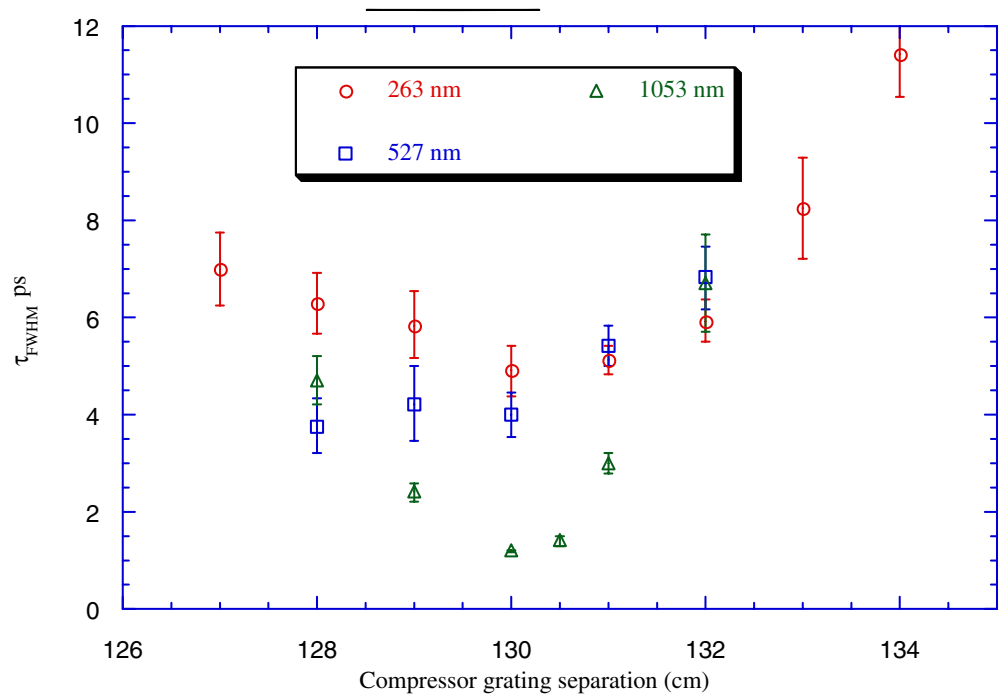


Figure 1: The IR, green and UV FWHM pulse lengths are plotted as a function of the compressor grating separation.

Figure 2 shows a typical measurement of the 3 UV pulse widths used in the experiments. The pulse is very nearly Gaussian for the short pulses but shows significant structure for pulse lengths > 10 ps. This is possibly due to either clipping on the compressor retro-reflector or the small bandwidth acceptance in the non-linear crystals. A small amount of spectral clipping on a highly chirped pulse can produce the temporal pulse structure seen in Figure 2 as will be shown in Section 3.

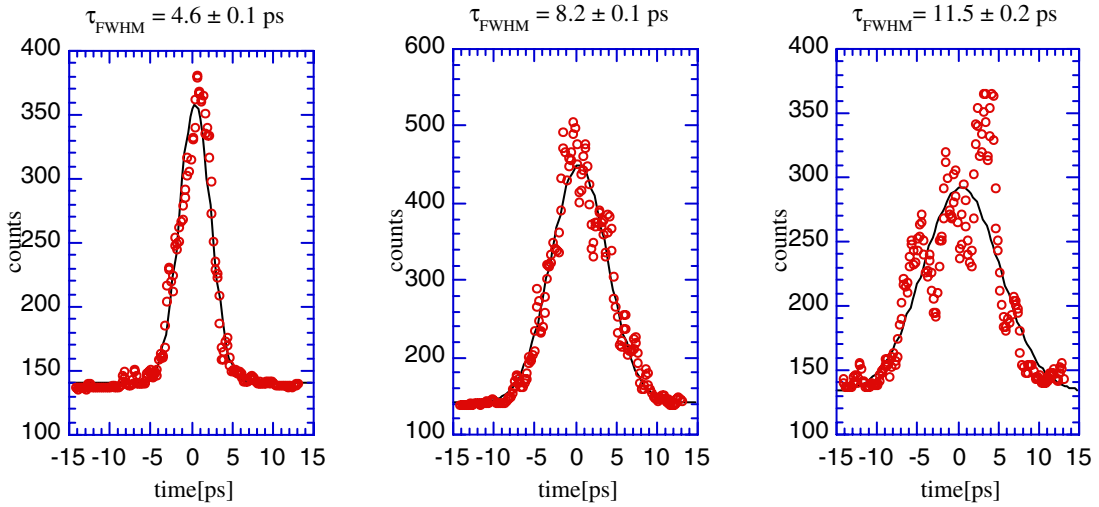


Figure 2: Typical streak camera output of the 5, 8 and 11 ps UV pulses along with a Gaussian fit.

The UV pulse is typically imaged onto the cathode at near normal incidence using an 8 m long 1:1 telescope. Grazing incidence is also possible and was used for the cleaning of the cathode described later in this section. Transverse shaping can be accomplished by imaging an aperture, after the quadrupling crystal, onto the cathode. The energy and transverse pulse shape incident on the cathode are measured by employing a 12 degree wedge pair less than 1 m from the cathode to pick-off two beams containing <10 % of the beam energy and send them to an energy meter and UV camera placed at the same distance from the beam pick-off as the cathode. This so called "virtual cathode" allows transverse pulse shape measurements on a shot to shot basis. The 263 nm laser pulse is incident at near normal incidence on the cathode from a 45 degree

Aluminum (90% reflectivity) mirror mounted in the vacuum system after traveling through a 90% transmissive vacuum window.

## 2.2 Timing jitter

Synchronization between the laser and the accelerator rf system is achieved by operating the laser at the 24th sub-harmonic of the 2856 MHz accelerator frequency. There is no feedback system controlling the laser repetition rate. Low timing jitter has been achieved by using a 125 MHz photo-diode to sample the pulse train from the laser oscillator as a master clock signal and frequency multiplying the signal after additional filtering in a phase-locked multiplier to generate the 2856 MHz rf signal. The output of the frequency multiplier is amplified to 1 kW, split and then fed to the two klystrons powering the rf gun and 3 m SLAC linac section. In this manner the accelerator rf is slaved to the frequency multiplied laser repetition rate instead of slaving both the laser and accelerator rf to an external reference source.

Typical measurements of the timing jitter at the GTF were conducted using a double balanced mixer as a phase bridge to measure shot to shot variations in the phase of different rf signals. The phase of the frequency multiplier, 1 kW amplifier, klystron and rf gun were measured and the result is plotted in Figure 3 where the plotted phases and rms jitter values are measured relative to the frequency multiplier output. The jitter in the rf gun measured over several minutes was 0.5 ps rms with negligible contributions from the klystron and the 1 kW amplifier. It is believed that this jitter is dominated by a shot to shot change in the difference between the master clock frequency and the standing wave gun resonant frequency which could be produced from either 100 Hz noise in the laser oscillator cavity length or 0.1 degree Celsius change in the gun temperature.

Acoustic noise on the laser table at 10 Hz and its harmonics up to ≈ 200 Hz has been measured using an accelerometer. The dominant source of this noise is the 10 Hz SSRL booster magnet supply located 2 m from the laser room. An additional noise source is evident at 60 Hz noise and its harmonics and is possibly due to the building air conditioning. The gun temperature variation has been measured with a thermocouple probe to be ± 0.2 degrees Celsius over the course of approximately half an hour. Due to the long time constant for the gun temperature variations, the most likely source of this jitter is the laser repetition rate variation.

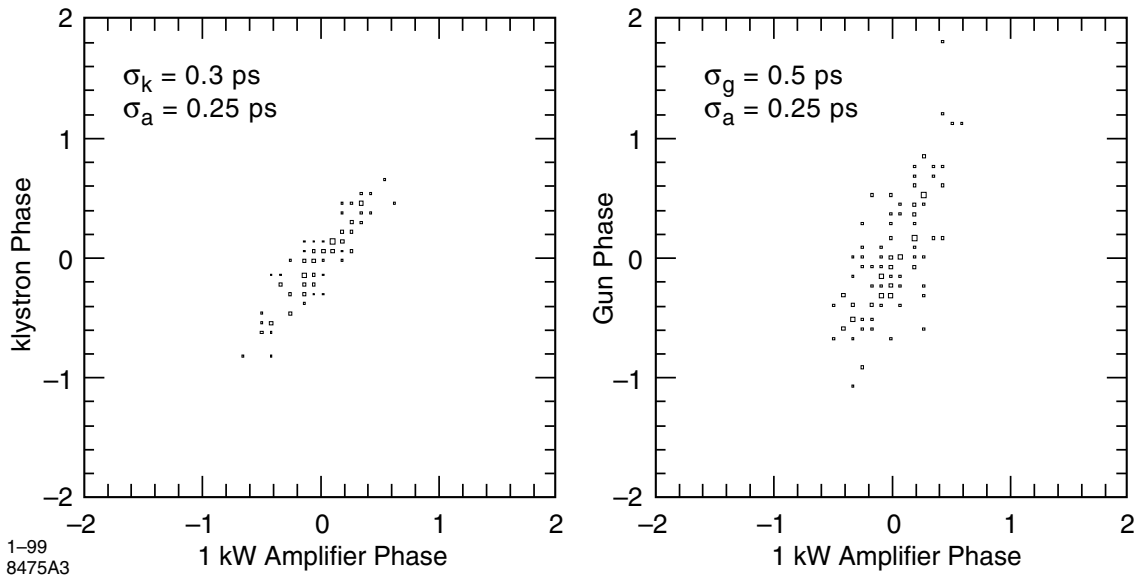


Figure 3: The shot to shot phase jitter of the GTF rf system is plotted in degrees where each phase is measured relative to the laser derived master clock.

The jitter between the 2856 MHz master clock and the 119 MHz from the laser was measured with a Tektronix 11801B digital sampling scope and found to be stable to ≤ 2 ps rms using the 119 MHz signal to trigger the oscilloscope while monitoring the

2856 MHz signal. The upper limit is set by the trigger jitter of the scope as measured by splitting the 119 MHz signal and using the outputs for both monitoring and triggering. The phase jitter in the phase-locked frequency multiplier was measured by measuring the frequency spectrum as outlined by Weingarten[6] et al. The 119 MHz input used for this measurement was a HP 8662A low phase noise rf source and the frequency multiplier output spectrum was measured with an HP spectrum analyzer with 1 kHz resolution bandwidth. The analysis revealed < 0.5 ps rms jitter due to the phase locked frequency multiplier. Finally, the amplified laser pulse demonstrated < 2 ps rms jitter by phase comparing the bandpass filtered output of a photodiode to the 119 MHz laser derived signal using a double balanced mixer. While no direct measurement of the UV laser pulse arrival time jitter at the cathode has been made, we can estimate the jitter to be < 3 ps rms (assuming the above measurements are not correlated). However, the long term drift between the laser and the gun can be on the order of tens of ps in the course of a day. In principle this could be eliminated with a slow feedback system on the laser cavity length, the gun temperature, or on the laser injection phase.

## 2.3 Quantum efficiency and thermal emittance

The electron yield/photon was measured using a Faraday cup located immediately downstream from the emittance compensation solenoid. Assuming a 100% collection efficiency by the Faraday cup this is equivalent to the quantum efficiency. As shown in Figure 4, the copper cathode in the GTF rf gun exhibited a very low quantum efficiency ($\approx 5\ 10^{-6}$ electron/photon) and large scale ($\approx 100\%$) non-uniformity. Therefore we elected to clean the cathode *in-situ*. A relatively high intensity ($\approx 2\ 10^{9}$ W/cm$^2$) laser pulse was incident on the cathode in the presence of $\approx 100$ MV/m electric field after

attempts to clean the cathode without the presence rf power failed. During the cleaning process $\approx 1$ μC of charge is extracted from the cathode in $\approx 50$ ns depleting the stored energy in the gun. The enhanced emission during this process appears to be the same explosive emission as previously reported[7] and was achieved by focusing the laser onto the cathode to an area roughly 1 mm x 0.3 mm at grazing incidence. The cathode was "cleaned" by continuously scanning the laser across an area 5 mm x 3 mm along the short axis of the laser at a rate of 22 shots/mm while maintaining the enhanced emission throughout each pass and with an overlap of 0.3 mm between passes. The cleaning resulted in a significant increase in the quantum efficiency and more uniform photo-emission as shown in Figure 4. However, the current due to field emission from the cathode also increased by roughly an order of magnitude. The increase in field emitted current is likely caused by areas of increased localized field due to a micro-roughening of the cathode surface after the explosive emission. It is believed that the increase in the

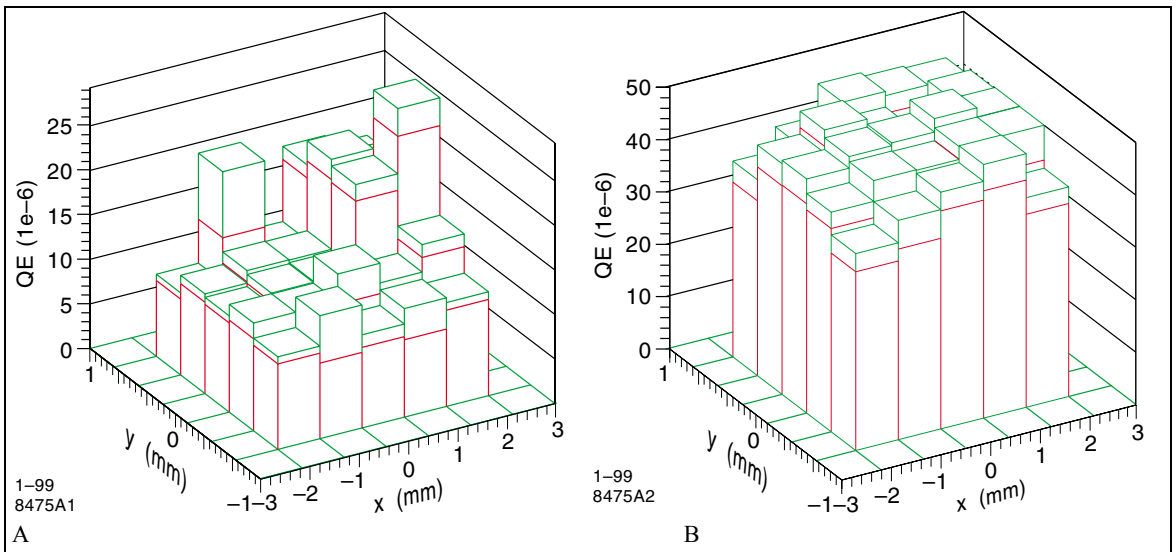


Figure 4: The measured quantum efficiency (electrons/photon) is plotted for the copper cathode both before (A) and after (B) laser cleaning.

quantum efficiency may be from removal of oxides or other contaminants from the cathode surface as well as the increased localized fields. The field emitted current was diminished by approximately a factor of 2-3 after long term exposure to high power rf fields (rf processing).

The Schottky effect is evident in a scan of the quantum efficiency as a function of laser injection phase (Schottky scan) as shown in Figure 5. The phase reference is such that the 90 degree phase point is defined as the time of maximum field at the cathode. The data was obtained at a single solenoid setting for phases below 100 degrees, but due to a significantly decreased energy and increased energy spread, the solenoid had to be varied for phases above 100 degrees in order to optimize charge collection on the Faraday

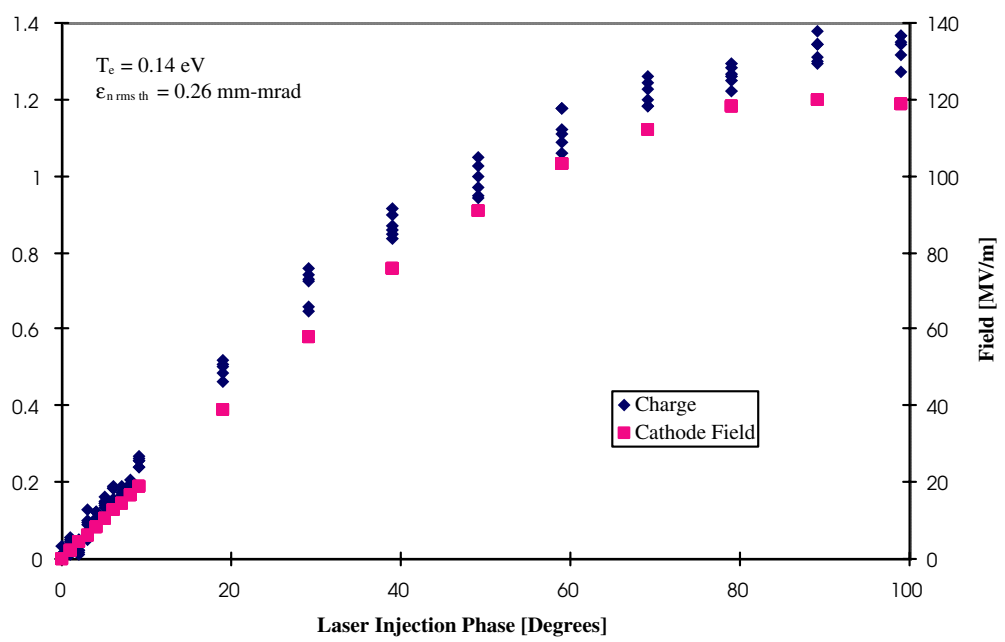


Figure 5: The measured charge extracted from the copper photo cathode with $\approx 190\ \mu J$ of laser energy and the rf field at the cathode are plotted as a function of injection phase.

cup. The scan is used to determine the absolute phase reference by observing where emission first takes place. Due to the finite duration of the laser pulse, the error in determining this reference phase is on the order of the pulse duration. For the measurements described in this paper, the zero phase was taken to be a few degrees into emission to correspond to the center of the bunch. The Schottky scan can also be used to determine the thermal emittance of the electron beam[8] which is the emittance of the electron beam exiting the cathode. For small changes in the cathode work function, the quantum efficiency varies exponentially as shown in Equation 1 where QE is the quantum efficiency, $\Delta\Phi$ is the change in the work function and $T_e$ is the effective temperature of the beam. The change in the work function due to the Schottky effect is shown in Equation 2 where $E_p$ is the peak field on axis at the cathode and $\theta$ is the laser injection phase. The temperature was estimated to be 0.14 eV from fitting the data in Figure 5 (although due to uncertainties in the charge collection, only data taken at phases $\leq$ 100 degrees are used in the calculation. The normalized rms thermal emittance for a transverse flat-top beam is shown in Equation 3 where $r_c$ is the beam radius and $m_0$ is the electron rest mass. For a 1 mm radius, the thermal emittance is calculated to be 0.2-0.3 $\pi$ mm-mrad which includes data from Schottky scans at several different values of peak field at the cathode.

$$QE \approx QE_o e^{\frac{\Delta\Phi}{kT_e}} \tag{1}$$

$$\Delta\Phi = \sqrt{\frac{e^3 E_p \sin\theta}{4\pi\varepsilon_o}} \tag{2}$$

$$\varepsilon_{n,rms,th} = \frac{r_c}{2}\sqrt{\frac{kT_e}{m_o c^2}} \tag{3}$$

## 2.4 Projected emittance

The horizontal emittance of the electron beam was measured downstream of the 3 m SLAC linac using the standard quadrupole scan technique whereby the beam size is measured on a screen downstream of a quadrupole which is varied so that the beam passes through a waist at the screen. The screen used was mounted at 45 degrees relative to the incident electron beam and was manufactured from SLAC chromate[9] which is a robust and reasonably sensitive material. The images were acquired with an 8-bit CCD Pulnix camera and Data Translation frame grabber both synched to the electron beam. The beam was focused to the smallest possible spot and an image was acquired. The image was then examined for saturation which was controlled by using a set of crossed polarizers between the lens and the camera. This allowed intensity control without changing the depth of field of the system. The lens used was a microscope objective with an adjustable zoom. A set of 127 um diameter wires on the screen were used for calibration purposes. The lens was set to give a calibration of 8 um per pixel to allow a compromise between capturing the full variation of the beam size and maximizing the resolution of smallest spot size. Once it was determined that the scan would be free of saturation the quadrupole was standardized. Five images of the beam and a background shot with the rf on but the laser off were taken at each quadrupole setting. In addition to the image of the electron beam, the following signals were recorded for each shot; the gun field level using a capacitive probe located by the vacuum pump out port in the gun's full cell, a Joule meter sampling the laser power incident on the cathode, the laser injection phase, the linac phase with respect to the gun and the beam charge using a

toroid. Quad scans were performed at various solenoid settings to try to find the magnetic field which produced the best emittance compensation[10] for a given set of running conditions. The background subtracted images of the beam were analyzed off line and the second moment of the beam profiles were calculated using the peak in the distribution as the center. The beam size versus quadrupole current for one of the scans is shown in Figure 6 along with the least square error fit from which the emittance is determined. Measurements were made with peak currents of up to 200 A at an energy between 25-35 MeV and simulations using the envelope equation with space charge[11] in the drift region

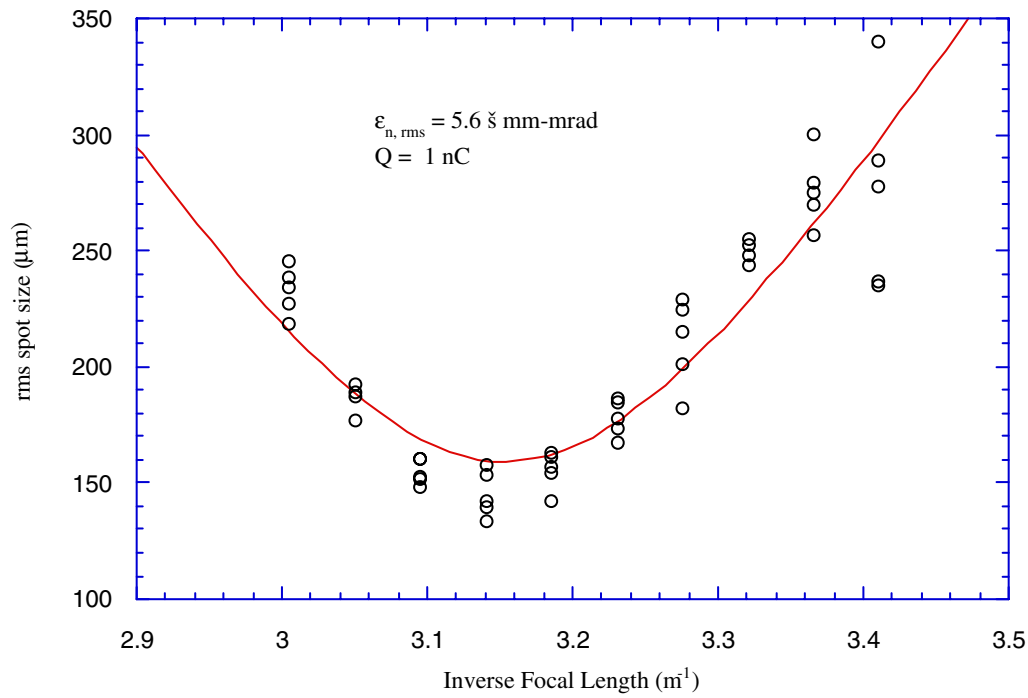


Figure 6: The measured rms spot sizes are shown as open circles and the fit is plotted as a solid line as a function of the inverse of the quadrupole focal length.

between the quadrupole and the screen have indicated no appreciable increase in the emittance due to space charge. Emittance growth due to space charge becomes noticeable with peak currents above 500 A at these energies, so no attempt was made to include space charge effects in the measured emittance presented here.

Emittance measurements were made with 1 nC of charge using a transverse Gaussian pulse with sigma's of 1.3 and 0.8 mm for x and y respectively, at a laser phase of 50 degrees, peak field on axis in the gun of 115 MV/m, and 10 degrees past the crest in the linac with a gradient of 9.7 MV/m. Lengthening the laser pulse from 5 ps FWHM to 8 ps FWHM reduced the normalized rms emittance from $8.3 \pm 0.7\ \pi$ mm-mrad at a solenoid field of 2.2 kG to $6.4 \pm 0.7\ \pi$ mm-mrad at a solenoid field of 2.0 kG respectively as shown in Figure 7. This is believed to be due to the reduction of space charge forces by lengthening the electron bunch. Measurements were also made with a laser pulse length of 11 ps FWHM which produced a normalized rms emittance of $6.6 \pm 0.2\ \pi$ mm-mrad at a solenoid field of 2.0 kG. However, only 0.7 nC of charge was available for this data so it is not directly comparable to the previous data. Additional measurements were made with the laser beam clipped at a radius of 1 mm although at a lower charge due to the loss of laser energy. The emittance results are shown in Table I along with the accelerator parameters used in the measurement. While these measurements were only performed once, individual quad scans which were repeated were consistent within the uncertainty of the measurement process.

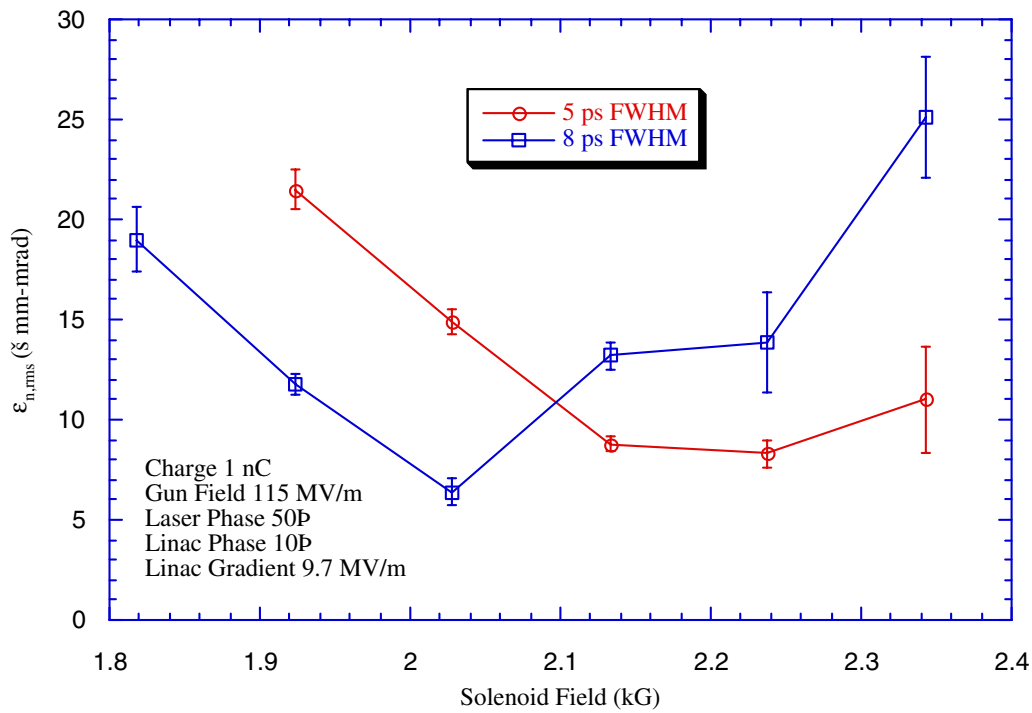


Figure 7: The emittance as a function of the solenoid field is plotted for both a 5 and 8 ps FWHM laser pulse.

The operating parameters for the data reported here were not optimum from theoretical considerations but were considered necessary from an operational point of view. Optimal emittance compensation is anticipated for fields around 140 MV/m[4]. However, the field in the gun was limited to 115 MV/m to reduce the amount of dark current emitted from the cathode to improve the signal to noise ratio for the beam size measurements. Also, the laser injection phase which produces the maximum charge emitted from the gun (see Figure 5) is not the same phase which produces a bunch with the maximum energy for a fixed field level in the gun and laser power on the cathode. The 1 nC data exhibits a structure in the energy distribution of the bunch displayed on a screen after a downstream spectrometer magnet. Low energy particles were displaced transversely with respect to those at higher energy resulting in a distribution with a

transverse kink. It is believed that this is due to the electron bunch traveling off center through the linac. The transverse displacement can be removed by steering through the linac, however, no studies have been made to date to determine if this actually improves the beam quality. PARMELA simulations indicate that for the present distance between the gun and linac the most efficient emittance compensation is achieved at a linac gradient of $\approx$ 6-7 MV/m yielding a final beam energy of $\approx$25 MeV. In fact the lowest emittance measured for 1 nC of charge shown in Figure 6 was 5.6 ± 0.5 $\pi$ mm-mrad at 6.3 MV/m at a laser injection phase of 60 degrees and solenoid field of 2.0 kG. However, it was found that for a higher gradient, the energy spread of the electron beam was smaller which made the determination of the phase of the bunch with respect to the RF in the linac more precise and so enabled greater repeatability when tuning the beam. Therefore, the linac gradient was chosen to be $\approx$10 MV/m for most of the measurements reported here despite the expected lower emittance at reduced linac gradients.

| $\varepsilon$ $\pi$ mm-mrad | Q nC | $\tau_{FWHM}$ ps | $\sigma_x/\sigma_y$ mm | $B_{sol}$ kG | Linac Field MV/m | Gun Field MV/m | Laser Phase degrees | Linac Phase degrees |
|---|---|---|---|---|---|---|---|---|
| 5.6 ± 0.5 | 1 | 5 ± 0.5 | 1.3/0.8 full | 2.0 | 6.4 | 115 | 60 | 10 |
| 8.3 ± 0.7 | 1 | 5 ± 0.5 | 1.3/0.8 full | 2.2 | 9.7 | 115 | 50 | 10 |
| 6.4 ± 0.7 | 1 | 8 ± 1 | 1.3/0.8 full | 2.0 | 9.7 | 115 | 50 | 10 |
| 6.6 ± 0.2 | 0.7 | 11 ± 1 | 1.3/0.8 full | 2.0 | 9.7 | 115 | 50 | 10 |
| 5.7 ± 0.2 | 0.4 | 5 ± 0.5 | 1.3/0.8 full | 2.0 | 9.7 | 115 | 50 | 10 |
| 6.3 ± 0.4 | 0.4 | 5 ± 0.5 | 1.0/1.0 clipped | 2.0 | 9.7 | 115 | 50 | 10 |
| 8.6 ± 0.4 | 0.4 | 8 ± 1 | 1.0/1.0 clipped | 1.9 | 9.7 | 115 | 50 | 10 |

Table 1: The measured normalized rms emittance and other relevant accelerator parameters are listed. The laser phase is referenced to the zero crossing in the gun while the linac phase is referenced to the crest in the 3 m SLAC linac.

## 3. LASER AND DIAGNOSTIC UPGRADE

Currently most of GTF laser system is being upgraded as 75% of the laser components described in this paper have been returned to collaborators. A new oscillator has already been installed which is an identical GLX-200 from Time-Bandwidth Inc. described earlier with a feedback system to lock the laser repetition rate to an external source. The rms timing jitter of the oscillator repetition rate with respect to the low phase noise reference source (HP 8662A) has been measured to be < 0.5 ps rms with the feedback system on and no attempt to reduce the acoustic vibrations on the laser table. While the laser will now be locked to an external clock, the rf system will still be slaved to the oscillator pulse train frequency. However, the external clock should eliminate the laser repetition rate variation which was evident in the RF gun phase jitter measurements shown in Figure 3. In addition a direct measurement of the timing jitter of the gun relative to the laser is planned using a fast photodiode (> 2856 MHz) and a double balanced mixer.

A new regenerative amplifier will also be installed. The new amplifier is expected to produce 5 mJ at 1054 nm at a 2.5 Hz rep rate. When the amplifier is installed the compressor will be realigned to remove the spatial chirp evident in the streak camera measurements. At the same time new doubling and quadrupling crystals will be installed that are matched to the IR intensity to prevent pulse lengthening seen in Figure 1 so that pulses as short as 1-2 ps FWHM can be generated in the UV. An adjustable telescope will also be installed so the laser spot size incident on the cathode can be varied. This will allow emittance measurements as a function of laser spot size.

According to simulation, in order to achieve a normalized emittance of 1 $\pi$ mm-mrad at 1 nC required by the LCLS, temporal and transverse laser pulse shaping is

required[4]. Both frequency domain and temporal domain pulse shaping experiments are being designed. Initial frequency domain pulse shaping will be achieved by hard edged bandwidth filters located in the optical compressor. Only a small amount of laser energy need be clipped when using a highly chirped beam to produce a significant flatter pulse with less than 5% ripple as shown in Figure 8. This pulse shaping would be performed in the IR so the effects of the doubling and quadrupling crystals still need to be considered. An alternative is a time domain technique based on a Michelson interferometer pulse stacker similar to that reported elsewhere[12]. Adjacent pulses will be orthogonally polarized to avoid interference effects and separated by approximately the pulse duration to produce a flat top pulse. This method will effectively allow one to sum the pulse intensities instead of the field since the interference between each identically polarized beam will be negligible.

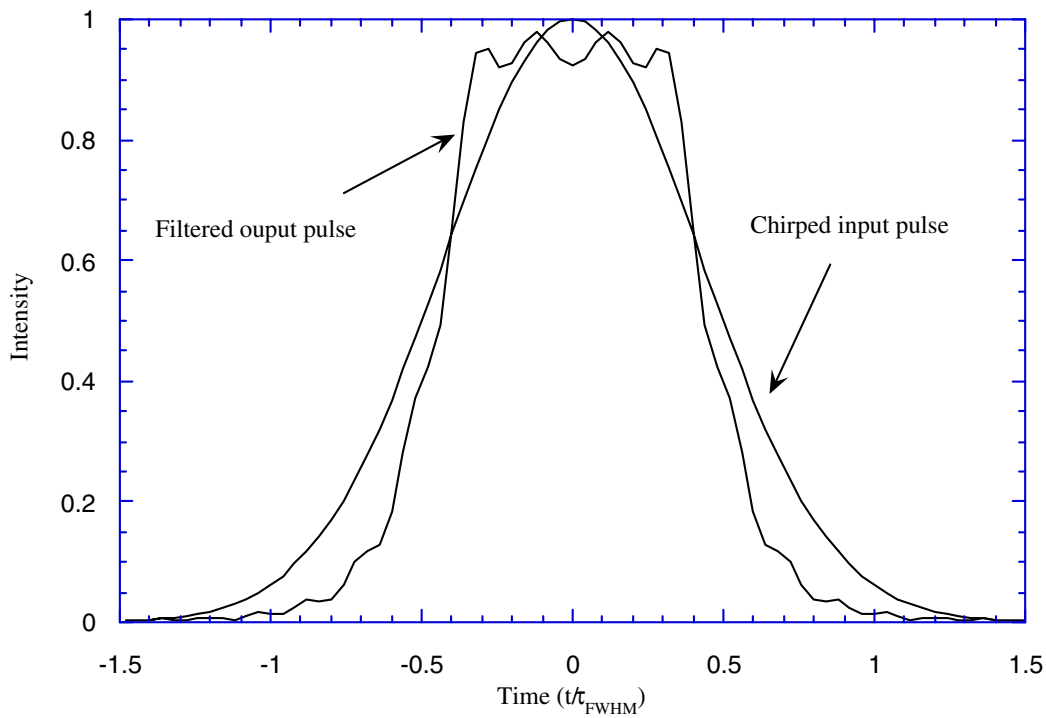


Figure 8: Laser pulse intensity vs. normalized time is plotted for a chirped pulse with a pulse length 10 times transform limited and the same pulse frequency filtered at ± 0.7 $\Delta\nu$.

Electron beam diagnostics are also being upgraded so that the full 6D phase space can be measured as well as to reduce measurement errors. We are currently replacing the phosphor screens with normal incidence Yttrium:Aluminum:Garnet (YAG) screens[13]. Optical radiation in the visible spectrum is extracted with polished Aluminum mirrors at 45 degrees located immediately downstream of the screens. The YAG screens have significantly smaller resolution <10 μm and also produce more light than the SLAC chromate. In addition, an Optical Transition Radiation (OTR) screen will be installed which can be used to measure the bunch longitudinal profile using a streak camera and

may also be used to measure the slice emittance[14]. A coherent OTR screen can also be used to measure the electron beam bunch length[15]. Quadrupole scan emittance measurements will also be cross checked using 2 or 3 screen emittance measurements. Finally a collimating slit will be installed after the spectrometer magnet so that the energy spread can be accurately quantified as well as measuring the longitudinal bunch profile by changing the phase of the linac to produce a linear dependence of particle arrival time on transverse position at the slit[16].

## 4. CONCLUSIONS

In summary we have completed emittance measurements with 1 nC of charge with 5 and 8 ps FWHM Gaussian laser pulses. The 8 ps pulse had 25% lower emittance and was optimized at a lower solenoid setting than the 5 ps long pulse with other accelerator parameters identical. The lowest emittance measured to date at the GTF with 1 nC of charge is 5.6 $\pi$ mm-mrad using a 5 ps long laser pulse and transverse and longitudinal Gaussian pulse shapes. The data agrees with PARMELA simulations and after adjusting for laser pulse length and transverse shape it also agrees with the 2.5-3.2 $\pi$ mm-mrad emittance measurements made at Brookhaven National Laboratory with an identical gun at 1 nC of charge[16].

The Nd:glass based GTF drive laser is currently delivering up to 200 mJ per pulse at 263 nm to the Cu cathode. A sub ps resolution streak camera was used to measure the 5-11 ps FWHM optical pulse length with nearly Gaussian pulse shapes. The timing jitter between the laser pulse and the rf system was measured to be < 3 ps. Temporal pulse shaping experiments are in progress which will enable the production of approximately flat-top laser pulses with 1-2 ps rise times and variable width. The particle tracking

code, PARMELA, predicts an emittance $\leq 1\ \pi$ mm-mrad with 1 nC of charge and a 10 ps flat-top pulse.

## 5. ACKNOWLEDGMENTS

The authors would especially like to acknowledge the work of the late Jim Weaver. Jim was instrumental in building the GTF rf gun as well as other components of the GTF. In addition we greatly appreciate the loan of the GLX-200 Nd:glass laser oscillator from Steve Milton at the APS and the Nd:glass regenerative amplifier head and Pockels' cells from David Meyerhofer and Adrian Melissinos at the University of Rochester. David Meyerhofer also provided valuable assistance with assembling and operating the laser system. We also appreciate the loan of the Hamamatsu FESCA-500 streak camera from Bob Siemann at SLAC and the A1976-01 UV optic set for the streak camera from Bill Cieslik of Hamamatsu. The rf gun currently under test at the GTF was part of the thesis work of Dennis Palmer at SLAC with contributions from Roger Miller at SLAC, X.-J. Wang at BNL and others. Finally we acknowledge Jym Clendenin, Max Cornacchia, Alan Fisher, Theo Kostseroglou, and Dennis Palmer at SLAC for useful discussions and the entire SSRL staff for assistance with assembly and operation of the GTF. This work was supported by the Department of Energy under contract number DE-AC03-76SF00515.

## 6. REFERENCES

1. M. Cornacchia et al, “LCLS Design Study Report”, www-ssrl.slac.stanford.edu/lcls
2. M. Cornacchia, “The LCLS x-ray FEL at SLAC”, these proceedings.

3. J.F. Schmerge et al, “SLAC RF photocathode gun test facility”, In SPIE *Free Electron Laser Challenges*, 2988, p. 90-96, San Jose, CA, 1997.

4. M. Hernandez et al, “Emittance measurements for the SLAC gun test facility”, In *IEEE Particle Accelerator Conference*, Vancouver, BC, 1997.

5. D.T. Palmer et al, “Emittance studies of the BNL/SLAC/UCLA 1.6 cell photocathode rf gun”, In *IEEE Particle Accelerator Conference*, Vancouver, BC, 1997.

6. M.J.W. Rodwell, “Subpicosecond laser timing stabilization”, IEEE Journal of Quantum Electronics, 25 (4), p. 817-827, 1989.

7. X.-J. Wang et al, “Intense electron emission due to picosecond laser produced plasmas in high gradient electric fields”, Journal of Applied Physics, 72 (3), p. 888-894, 1992.

8. J.E. Clendenin and G.A. Mulhollan, “High quantum yield, low emittance electron sources”, SLAC PUB , 1998.

9. S. Yencho and D.R. Walz, “A high resolution phosphor screen beam profile monitor”, IEEE Transactions, 32, p. 2009-2011, 1985.

10. B.E. Carlsten, “New photoelectric injector design for the Los Alamos National Laboratory XUV FEL accelerator”, Nuclear Instruments and Methods in Physics Research, Vol. A285, p. 313, 1989.

11. M. Reiser, *Theory and Design of Charged Particle Beams*, Wiley, New York, 1994.

12. C.W. Siders and A.J. Taylor, “High-energy pulse train and shaped pulse generator using a 100% throughput $2^n$-pulse Michelson interferometer”, in *Ultrafast Optics Conference*, Monterey, CA, 1997.

13. W.S. Graves, “A high resolution electron beam profile monitor”, In *IEEE Particle Accelerator Conference*, Vancouver, BC, 1997.

14. S. Gierman, Los Alamos National Laboratory, private communication, 1998.

15. H.-C. Lihn, “Measurement of 50-fs (RMS) electron pulses”, In *Beam Instrumentation Workshop*, 333, p. 231-237, Vancouver, BC, 1994.

16. M. Babzien et al, “Observation of self-amplified spontaneous emission in the near-infrared and visible wavelengths”, Physical Review E, 57 (5), p. 6093-6100, 1998.